Available online at www.sciencedirect.com
ScienceDirect
Electrochimica Acta 52 (2007) 3149–3159
ELECTROCHIMICA Acta
www.elsevier.com/locate/electacta

Performance of hybrid density functional theory methods toward oxygen electroreduction over platinum

Titus V. Albu *, Sean E. Mikel

Department of Chemistry, Box 5055, Tennessee Technological University, Cookeville, TN 38505, USA

Received 17 July 2006; received in revised form 22 September 2006; accepted 22 September 2006
Available online 27 October 2006

Abstract

The performance of a large number of hybrid density functional theory methods is evaluated toward calculating potential-dependent activation energies for uncatalyzed and Pt-catalyzed oxygen reduction and hydroperoxyl oxidation. This reaction is the first step and the rate-determining step in the electrochemical oxygen reduction, which is the cathodic process in electrolyte-based fuel cells. Special focus is put on determining methods that allow results comparable to those previously calculated using MP2 method with the 6-31G(d,p) basis set for O and H and the LANL2DZ basis set for Pt. This level of theory was shown to reproduce well, within the model used here, key features of experimental data. It is found that hybrid density functional theory methods with small (less than 30%) Hartree–Fock exchange contributions give less accurate results mainly due to underestimated calculated activation energies while methods with higher (around 50%) Hartree–Fock exchange contributions give results closer to the target ones. New hybrid density functional theory methods with specific reaction parameters that give superior results are proposed. The best overall performance is found for the method denoted as B1B95-50 in which the Hartree–Fock exchange contribution is half. This method is computationally affordable and offers promise as a reliable method in applications to larger systems.

Keywords: Oxygen reduction; Hydroperoxyl oxidation; Activation energy; Platinum; Density functional theory; Hartree–Fock exchange

1. Introduction

The need for an environmentally clean, highly efficient source of energy has generated a special interest in fuel cell development over the past few decades. A fuel cell converts energy produced in a chemical reaction into electricity with better efficiency than other methods. An important goal for basic research and for the development of practical portable electric power sources in the form of hydrocarbon-fed electrochemical fuel cells is the understanding of the factors governing the electrode processes. The biggest problem in the fuel cell industry is the cathodic process of oxygen reduction because of its very slow kinetics leading to a high overpotential (i.e., cathodic voltages that are less positive than the reversible potential) and high current flows only at potentials with lower technological interest.

For acid-electrolyte fuel cells, the best electrocatalysts for the oxygen reduction reaction (ORR) are platinum and its alloys. Several studies on platinum alloys with transition metals such as Co, Cr, Ni, V, Ti, etc., have shown enhanced electrocatalytic activity for ORR with respect to Pt alone [1–8]. This improvement has been attributed to different structural changes caused by alloying: favorable Pt–Pt interatomic distanced [1,7,8], surface roughening caused by the dissolution of the more oxidizable components [2], the increase of the *d*-electron vacancy of a Pt surface layer covering the underlying alloy atoms [5], the existence of an ordered structure [3], or a combination of electronic and geometric effects [4,6]. The source of increased activity of Pt alloys toward ORR is somehow controversial in even more recent studies [9–15]. Paulus et al. [10,11] propose that the activity enhancement is contained in the pre-exponential factor of the transition state theory rate constant while Uribe and Zawodzinski [12] and Stamenkovic et al. [13,14] propose that the weaker adsorption of hydroxyl to the electrode surface, which frees more of the surface for ORR, is actually responsible for it. As suggested in some of these experimental studies [13,14], theoretical studies should bring a better understanding of the energetics of chemisorbed species on the surfaces of these alloys as well the factors responsible for the enhanced activity of platinum alloys.

* Corresponding author. Tel.: +1 931 372 6324; fax: +1 931 372 3434.
E-mail address: albu@tntech.edu (T.V. Albu).

0013-4686/$ – see front matter © 2006 Elsevier Ltd. All rights reserved.
doi:10.1016/j.electacta.2006.09.057

The number of theoretical studies concerning the ORR over platinum is still limited [16–25]. Anderson and Albu used MP2 calculations to determine the potential-dependent activation energies for the ORR over Pt with O_2 bonded end-on [17]. When compared to the outer-sphere ORR [26,27], the results show the catalytic effect of bonding to Pt. It was also postulated that the end-on bonding of O_2 to the electrode will lead to the two-electron reduction and formation of hydrogen peroxide while the bridge interaction will lead to the preferred four-electron reduction to water, and a follow-up, B3LYP study of ORR over a Pt dual site supported this assumption [18]. The MP2 calculations were computationally prohibited for larger reactive models that include more Pt atoms. Different approaches in investigating the first electron-transfer step in ORR, which has been well established to be the rate-determining step, were used in theoretical studies by Hartnig and Koper [19], Li and Balbuena [20], and Wang and Balbuena [21–24]. Few recent theoretical studies examine oxygen species chemisorbed on platinum and platinum alloys using cluster [28–31] or slab [32–37] calculations, but these studies focused more on the energetics and electrode coverage and less on the dynamics of electrochemical oxygen reduction. The current status of the quantum mechanical studies of ORR, including O_2 chemisorption on fuel cells catalysts, has been recently reviewed in more detail by Shi et al. [38].

Hybrid density functional theory (HDFT) methods are the most popular electronic structure theory methods for large molecules and molecular clusters because they are computationally affordable and yield accurate molecular properties like geometries, vibrational frequencies, and enthalpies of formation. Some of these methods fail however to perform well in the transition-state region where bond breaking and forming occur. By optimizing existing methods against kinetics data, new HDFT methods for use in kinetics studies have been developed [39–41]. These methods provide more accurate barrier heights and a better description of the potential energy surface (PES) in the transition state region.

In the present work, the results of an investigation on the energetics of the first step of ORR in acidic media, both uncatalyzed (or outer-sphere) and Pt-catalyzed are presented. The chemical equations for these reactions are below.

$$O_2 + H^+(aq) + e^-(U) \rightarrow HOO \quad (1)$$

$$Pt\text{–}O_2 + H^+(aq) + e^-(U) \rightarrow Pt\text{–}OOH \quad (2)$$

The calculations were carried out with a large number of HDFT methods. One purpose of this study is to carry out a comparative study involving various HDFT methods that will allow a suitable interpretation of results obtained on ORR by different authors using different methods. The other purpose of the study is to determine HDFT methods that give results similar to the MP2 results of previous studies [26,17], and new methods are developed and proposed for use in studies of oxygen electroreduction on large platinum clusters.

2. Computational methodologies

2.1. Local reaction center electron-transfer theory

In local reaction center electron-transfer theory, an electrochemical reaction is taking place when the reaction center (i.e., a model for the reaction center) has the ability, due to thermal fluctuations in its geometry, to either accept (if reduction is modeled) or donate (if oxidation is modeled) an electron from an electrode at a certain potential. Radiationless electron transfer is assumed between the electrode and the reaction center. The chemical potential, μ, of electrons at the surface of a metallic electrode is the Fermi energy and is equal to the negative of the thermodynamic work function of the surface, φ. On the standard hydrogen electrochemical scale, the electrode potential U (V) is given as:

$$U\,(\mathrm{V}) = \varphi\,(\mathrm{eV}) - \varphi_{H^+/H_2}\,(\mathrm{eV}) \quad (3)$$

where φ_{H^+/H_2} is the thermodynamic work function of the standard hydrogen electrode. In this work, the average value of 4.6 eV has been used for φ_{H^+/H_2} [42].

In modeling an electrochemical reaction, because the electrode is acting just as an electron donor or acceptor, it is preferred to replace the electrode by a smaller (i.e., computationally easier to model) non-interacting electron donor/acceptor. The only condition is that the electron donor (or acceptor) will have an ionization potential (or electron affinity) that matches the thermodynamic work function of the electrode. For example, for studying hydrogen evolution from diamond electrodes, a Li atom has been used as an electron donor [43]. An even more convenient way to model the electrode at a certain potential is to include only the energy of the electron (assumed to come from or go to the electrode) on the vacuum scale of energies. In this case:

$$U\,(\mathrm{V}) = E_{e^-}\,(\mathrm{eV}) - 4.6 \quad (4)$$

where E_{e^-} is the energy of the electron on the vacuum scale. Fig. 1 shows the relationship between the electrochemical scale of potentials and the vacuum scale of the energies, assuming the 4.6 value for φ_{H^+/H_2}. In this figure, an electrode at 0.7 V on the standard electrochemical scale will have a thermodynamic

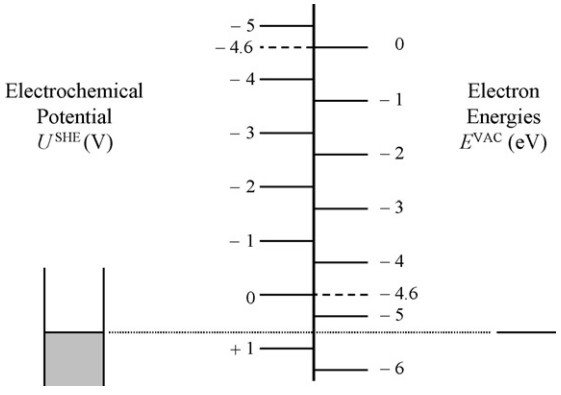

Fig. 1. Relationship between the standard-hydrogen-electrode scale of electrochemical potentials and the vacuum scale of energies.

work function of 5.3 eV that is equivalent with the Fermi level at −5.3 eV. The electrons coming from or going to this electrode will have energy of −5.3 eV on the vacuum scale, and these electrons are represented in Fig. 1 as the level at that energy on the vacuum scale. The smaller (i.e., less positive) the electrochemical potential of an electrode, the higher (i.e., less negative) the electron energy coming from its Fermi level.

For a reduction reaction, as is the ORR case investigated here, the oxidized form of the reaction center (Ox) needs to be thermally activated to be able to accept the electron with a certain energy (E_{e^-}) and become the reduced form of the reaction center (Red):

$$Ox^* + e^-(E_{e^-}) \rightleftharpoons Red^* \quad (5)$$

where asterisk (*) indicates that the reactant center is in a thermally activated structure both in the oxidized and the reduced form. It is evident that the reaction center structures in the oxidized form that can be reduced by an electron with a particular E_{e^-} are only the structures that have an electron affinity equal to the electron energy in the absolute value. All the other structures will not allow a radiationless transition of an electron with that energy.

Investigating the electron-transfer state for an electrochemical reduction reaction at a certain potential becomes therefore a search for structures of the reaction model that have the same electron affinity. This is equivalent to locating the crossing region of two potential energy surfaces (i.e., the reactant and product energy surfaces) representing two different electronic states. In the reduction example above, the reactant surface is given by ($E_{Ox^*} + E_{e^-}$) while the product surface is given by E_{Red^*}. A representation of these two surfaces for three different electrode potentials is shown in Fig. 2. On one of these electrode potentials, $U_{red=0}$, the reduction process is barrierless and the crossing of the two surfaces includes the minimum of the Ox surface. For another electrode potential, $U_{oxi=0}$, the oxidation process is barrierless and the crossing of the two surfaces includes the minimum of the Red surface. Finally, the middle electrode potential is the reversible potential, where the two states (oxidized and reduced) are in equilibrium. In this case, the electron-transfer state is not a stationary point on either one of the surfaces.

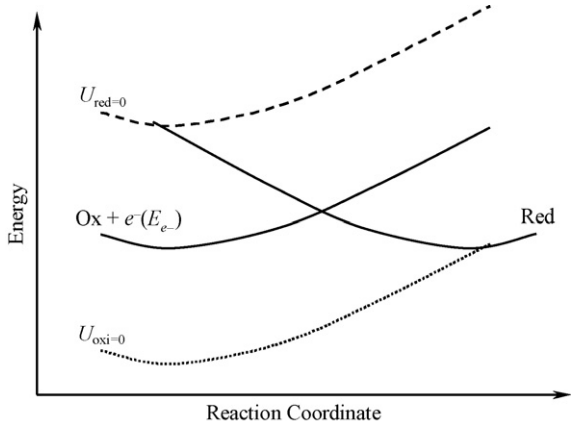

Fig. 2. Schematics of diabatic potential energy surfaces for the reduced (Red) and oxidized (Ox) form of the reaction center in an electron-transfer process and the potential dependence of the oxidized form when considering the electron energy.

Generally, for a system of $3N-6$ internal coordinates (as is the case of a reactive system containing N atoms), the locus of points (or hypersurface) of constant electron affinity forms a $(3N-7)$-dimensional surface. The lowest energy structure on this hypersurface is generally assumed to be the electron-transfer state. In the original work [26,17,27], this pattern-search approach to determining the electron-transfer state was a tedious, time-consuming, and computationally demanding procedure, and was limited to only a few of the $3N-7$ degrees of freedom of the hypersurface. More recently, a computer program to do this search automatically, using the Lagrange method of undetermined multipliers, was written and tested successfully on Pt–OH_2 oxidation [44].

A significant parameter for understanding catalysis is the activation energy, which is directly related to the classical barrier height, i.e., the energy difference between the energy of the transition state (or more precisely, the saddle point) and the energy of reactants (or of a reactant complex). For all the systems investigated in this study, and in most if not all the other systems investigated with this methodology, the electron-transfer state is the highest energy state along the reaction coordinate, and it therefore coincides with the transition state. This should not necessarily be true for other systems. Once the electron-transfer state (i.e., the transition state) is located, the barrier height (which was called activation energy in previous studies and will be called the same in the rest of this paper) is determined as the energy difference between the energy of the transition state and the energy of the van der Waals complex formed by reactants. This diabatic activation energy is an upper limit to the adiabatic activation energy. In the present level of modeling, zero-point energy contributions are not included. The complex formed between the reactants of a reduction reaction is a minimum on the Ox potential energy surface and is called the reduction precursor. Similarly, the complex formed between reactants of an oxidation reaction is a minimum on the Red potential energy surface and is called the oxidation precursor.

The theory, latest advances, and some of its applications have been recently reviewed in more detailed by Anderson [45] and Anderson et al. [46].

2.2. Reaction center model

The reaction center model used in this study is essentially identical to the one used in previous studies of uncatalyzed [26,27] and Pt-catalyzed [17] oxygen reduction, and it will be just briefly introduced here. A representation of this model is shown in Fig. 3 for the case of Pt-catalyzed ORR. The hydronium ion in solution is modeled by a hydronium ion solvated with two water molecules, $(H_2O)_2H_2O$–H^+, having C_s symmetry. For each HDFT method investigated, after the initial optimization at that level of theory, the $(H_2O)_2H_2O$ part is kept rigid and only the O–H^+ distance is allowed to change during optimizations and activation energy determinations. The optimization of the reduction and oxidation precursors as well as the

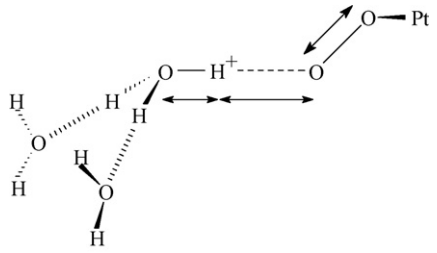

Fig. 3. Reaction model and the variables changing during the reduction or oxidation process.

transition state search is therefore done in a three-dimensional space, and the only distances that are allowed to vary are O–H^+, $H^+\cdots O_2$, and O–O, as defined in Fig. 3. The O–$H^+\cdots O_2$ part is kept linear for both uncatalyzed and Pt-catalyzed ORR. For uncatalyzed ORR, the $H^+\cdots$O–O angle is kept fixed at the optimized value in hydroperoxyl. For Pt-catalyzed ORR, the Pt–O distance, the Pt–O–O angle, the $H^+\cdots$O–O angle, and the $H^+\cdots$O–O–Pt dihedral are kept fixed at the optimized PtOOH values.

2.3. Hybrid density functional theory methods

In hybrid density functional theory methods, the one-parameter hybrid Fock–Kohn–Sham operator can be written as:

$$F = F^{H} + \left(\frac{X}{100}\right) F^{HFE} + \left[1 - \left(\frac{X}{100}\right)\right](F^{SE} + F^{GCE}) + F^{C} \quad (6)$$

where F^H is the Hartree operator (i.e., the non-exchange part of the Hartree–Fock operator), F^{HFE} the Hartree–Fock (HF) exchange operator, X the fraction of Hartree–Fock exchange, F^{SE} the Dirac–Slater local density functional for exchange, F^{GCE} the gradient correction for the exchange functional, and F^C is the total correlation functional including both local and gradient-corrected parts.

The existing HDFT methods (i.e., HDFT methods present in the literature) used in this study are B3LYP [47,48], BH&HLYP [47,48], B3PW91 [48], PBE1PBE [49], mPW1PW91 [50], MPW1K [39], B1B95 [51], BB1K [40], mPW1B95 [41], and MPWB1K [41]. In addition, we developed and used new HDFT methods in which the X value is different than the value in generic methods. The names of these new methods are based on the original HDFT method from which they were derived but include the non-standard value of X. The HDFT methods obtained for non-standard values of X are labeled in this study by defining the gradient-correlated exchanged functional used, followed by 1 indicating a one-parameter method, followed by the correlation functional used, and finally by the value of X separated by a dash. For example, mPW1B95-50 represents a one-parameter hybrid density functional theory method based on the modified Perdew–Wang (mPW) gradient-corrected exchange functional [50] and B95 gradient-corrected correlation functional [51], and with a Hartree–Fock exchange contribution of 50% ($X = 50$).

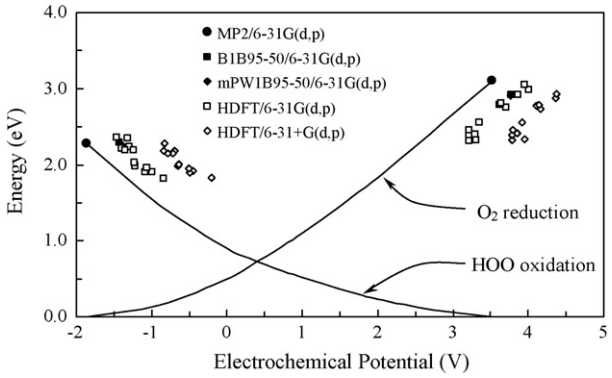

Fig. 4. Calculated activation energies vs. the electrochemical potential for the uncatalyzed O_2 reduction and HOO oxidation.

2.4. Computational details

In the present study, 6-31G(d,p) and 6-31+G(d,p) basis sets were used for H and O and the effective core potential LANL2DZ basis set was used for Pt. The geometry optimizations were carried out using tight convergence criteria, and an ultrafine integration grid was used for numerical integrations. Restricted wave functions were used for closed-shell systems and unrestricted wave functions for open-shell systems. For the reaction systems containing platinum, in order to ensure that the lowest energy spin state is determined, different electronic configurations (i.e., orbital occupations) were investigated. All electronic structure calculations were carried out using Gaussian 03 program [52].

3. Results

The results of our calculations are given in two tables, and additional results are presented as Appendix A. Table 1 contains the calculated reversible potential for oxygen reduction to water, the electrochemical potentials of barrierless reactions, and selected activation energies. This table contains the MP2/6-31G(d,p) results, the results obtained with various HDFT methods, and the calculated errors for the HDFT methods when compared with the MP2 results as described below. Table 2 contains similar results obtained for Pt-catalyzed oxygen reduction and hydroperoxyl oxidation with only a subset of HDFT methods. The results are shown in two figures. Fig. 4 shows the results for the uncatalyzed oxygen reduction and hydroperoxyl oxidation, and Fig. 5 shows the results for the Pt-catalyzed oxygen reduction and hydroperoxyl oxidation.

4. Discussion

In the first part of our study, a large number of HDFT methods were investigated toward the uncatalyzed oxygen reduction reaction. The results were compared with those obtained with the MP2/6-31G(d,p) method. It was found in previous studies [26,27] that this method provides, within the reaction model used there (and here), nearly quantitative results in terms of calcu-

Table 1
Hartree–Fock exchange contribution X, calculated reversible potential for $O_2 + 4H^+ + 4e^- \rightleftharpoons 2H_2O$ reaction, electrochemical potentials and activation energies for $O_2 + H_3O^+ + e^- \rightleftharpoons OOH + H_2O$ reaction, and the average error relative to the MP2/6-31G(d,p) results

Basis set/HDFT method	X	U°	$(U)_{E_a^{red}=0}$	$(E_a^{oxi})U_{red=0}$	$(U)_{E_a^{oxi}=0}$	$(E_a^{red})U_{oxi=0}$	Error
MP2/6-31G(d,p)		1.12	−1.867	2.278	3.513	3.102	0.00
6-31G(d,p)							
B3PW91	20	1.12	−0.998	1.907	3.221	2.312	0.89
B3LYP	20	1.20	−0.837	1.816	3.301	2.322	0.97
BH&HLYP	50	1.24	−1.293	2.233	3.865	2.925	0.48
PBE1PBE	25	1.03	−1.084	1.910	3.213	2.387	0.82
mPW1PW91	25	1.10	−1.069	1.958	3.296	2.406	0.80
MPW1K	42.8	1.22	−1.240	2.193	3.708	2.755	0.52
mPW1PW91-60	60	1.32	−1.318	2.345	4.010	2.983	0.53
B1B95	28	1.06	−1.225	1.984	3.211	2.452	0.71
BB1K	42	1.17	−1.395	2.216	3.614	2.793	0.40
B1B95-50	50	1.22	−1.436	2.289	3.778	2.924	0.38
B1B95-60	60	1.28	−1.464	2.363	3.950	3.051	0.43
mPW1B95	31	1.08	−1.233	2.023	3.345	2.554	0.63
MPWB1K	44	1.16	−1.351	2.188	3.643	2.806	0.42
mPW1B95-50	50	1.20	−1.387	2.247	3.764	2.904	0.40
6-31G+(d,p)							
B3PW91	20	1.92	−0.448	1.913	3.787	2.323	1.15
B3LYP	20	2.08	−0.207	1.828	3.952	2.331	1.30
BH&HLYP	50	2.00	−0.695	2.178	4.361	2.878	1.03
PBE1PBE	25	1.83	−0.500	1.891	3.783	2.392	1.09
mPW1PW91	25	1.89	−0.506	1.948	3.852	2.410	1.09
MPW1K	42.8	1.91	−0.715	2.152	4.166	2.729	0.96
mPW1PW91-60	60	1.94	−0.833	2.283	4.377	2.927	0.96
B1B95	28	1.87	−0.650	1.981	3.791	2.461	0.98
BB1K	42	1.90	−0.845	2.178	4.111	2.778	0.85
mPW1B95	31	1.89	−0.637	2.002	3.920	2.555	0.97
MPWB1K	44	1.90	−0.782	2.144	4.147	2.786	0.90

The electrochemical potentials are in V, and the activation energies are in eV.

Table 2
Electrochemical potentials and activation energies for $Pt–O_2 + H_3O^+ + e^- \rightleftharpoons Pt–OOH + H_2O$ reaction, and the average error relative to the MP2/6-31G(d,p) results

HDFT method	$(U)_{E_a^{red}=0}$	$(E_a^{oxi})U_{red=0}$	$(U)_{E_a^{oxi}=0}$	$(E_a^{red})U_{oxi=0}$	Error
MP2/6-31G(d,p)[a]	0.382	1.330	2.681	0.969	0.00
B3PW91/6-31G(d,p)	0.929	0.529	2.280	0.822	0.70
BH&HLYP/6-31G(d,p)	0.493	0.846	2.651	1.312	0.42
MPW1K/6-31G(d,p)	0.633	0.762	2.651	1.256	0.45
mPW1PW91-60/6-31G(d,p)	0.470	0.904	2.709	1.335	0.40
B1B95-50/6-31G(d,p)	0.451	0.877	2.636	1.307	0.40
mPW1B95-50/6-31G(d,p)	0.475	0.862	2.661	1.324	0.42

The electrochemical potentials are in V, and the activation energies are in eV.
[a] The basis set used for platinum is LANL2DZ.

lated reversible potentials and relatively high activation energy calculated for uncatalyzed oxygen reduction. Also, the calculated activation energy for the first step of Pt-catalyzed oxygen reduction of 0.43 kcal/mol falls well within the experimental range of values of 0.2–0.5 eV [17]. The calculated value is essentially identical with the values of 0.44 and 0.45 eV obtained over the three low-index platinum surfaces in 0.05 M H_2SO_4 (aq) [53] and in pH 1.9 $HClO_4$ solution over polycrystalline platinum electrodes [54], respectively. The good accuracy obtained in these studies is probably unforeseen considering the relative small size of the reaction model and the electronic structure theory used, and probably includes a fortuitous cancellation of errors. (For example, the use of the larger 6-31+G(d,p) basis set used for oxygen, that can be seen as an advancement, gives much smaller and therefore less accurate activation energies for the uncatalyzed oxygen reduction [27].) Unfortunately, the MP2/6-31G(d,p)-LANL2DZ methodology becomes computational prohibited when applied to larger models that include more Pt atoms. As a result, one of the goals of this work is to determine HDFT methods that can reproduce closely the MP2

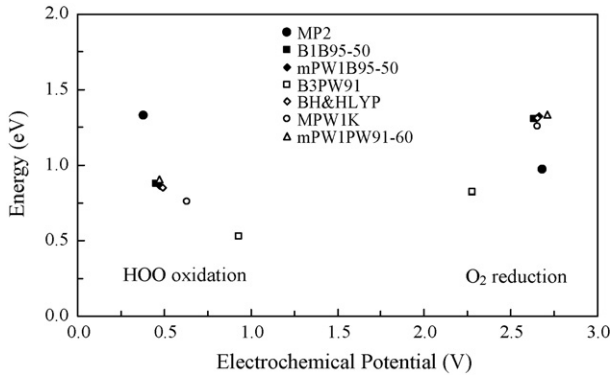

Fig. 5. Calculated activation energies vs. the electrochemical potential for the Pt-catalyzed O_2 reduction and HOO oxidation.

results and that can be applied with less difficulty to larger electrode models.

One calculated quantity with all HDFT methods is the reversible potential for the four-electron reduction of O_2 to water. For each HDFT method, this reversible potential was calculated based on:

$$U^\circ\,(\mathrm{V}) = -\frac{\Delta E}{4}\,(\mathrm{eV}) - 4.6 \tag{7}$$

where ΔE is the classical energy of reaction for the four-electron oxygen reduction process given by chemical equation:

$$O_2 + 4(H_2O)_2H_3O^+ + 4e^- \rightarrow 4(H_2O)_2H_2O + 2H_2O \tag{8}$$

where $(H_2O)_2H_3O^+$ is the hydronium ion solvated with two water molecules that is used in modeling the potential-dependent activation energy and $(H_2O)_2H_2O$ is the cluster of three water molecules having the same geometry as in $(H_2O)_2H_3O^+$. The calculated reversible potentials are given in Table 1. The experimental value of the reversible potential for ORR is 1.23 eV [55]. Inspecting the results in Table 1, one can easily see that most of the HDFT methods investigated here gives relatively accurate results in conjunction with the 6-31G(d,p) basis set while the values obtained with the larger 6-31+G(d,p) basis set are consistently overestimating the experimental value. Comparing only methods that differ not by the choice of functionals used but by the HF exchange contribution (e.g., B1B95, BB1K, B1B95-50, and B1B95-60), the calculated reversible potential increases with the HF exchange contribution.

A comprehensive study was also carried out for the potential dependence of the activation energy of uncatalyzed oxygen reduction and hydroperoxyl oxidation. In the model used here, the process of one-electron reduction of O_2 to HOO in acid solution requires that the reactants, oxygen and the solvated hydronium ion, come close to each other and form the hydrogen-bonded complex called reduction precursor, $(H_2O)_2H_2O$–$H^+\cdots$OO. The reduction activation energies are calculated with respect to the energy of this precursor. Similarly, for the reverse oxidation reaction, $(H_2O)_2H_2O$ and H–OO form a hydrogen-bonded oxidation precursor, $(H_2O)_2H_2O\cdots$H–OO. Structural parameters of these precursors are given in Appendix A. In this study, the oxidized form of the reaction model has a spin multiplicity of 3, and the reduced form of the reaction model has a spin multiplicity of 2.

Calculating the electron affinity of the reduction precursor allows one to determine, based on Eq. (4), the electrochemical potential at which the reduction becomes barrierless which is denoted $(U)_{E_a^{red}=0}$ in Tables 1 and 2 or $U_{red=0}$ in Fig. 2. This is true because, at that potential, the reduction precursor is the most stable structure with the calculated electron affinity. Similarly, calculating the ionization potential of the oxidation precursor, one can determine the electrochemical potential at which the oxidation becomes barrierless which is denoted $(U)_{E_a^{oxi}=0}$ in Tables 1 and 2 or $U_{oxi=0}$ in Fig. 2. The oxidation activation energy at the $U_{red=0}$, denoted $(E_a^{oxi})_{U_{red=0}}$, and the reduction activation energy at $U_{oxi=0}$, denoted $(E_a^{red})_{U_{oxi=0}}$, were also calculated and given in Table 1. Those four important quantities determine two points in the activation energy versus the electrochemical potential representation shown in Fig. 4. In this figure, the curves representing the activation energy dependence on the electrochemical potential were calculated previously at the MP2/6-31G(d,p) level of theory [26]. Instead of a broad study that would include the potential dependence of activation energy over a wide range of electrode potentials for each HDFT method, the comparison between the MP2 results and the HDFT results was made between only these two points. The MP2/6-31G(d,p) results obtained previously serve as the "target" results.

The accuracy of an HDFT method with respect to the MP2 results is calculated as the average of the generalized distances between the MP2 points and the HDFT points in the activation energy versus the electrochemical potential representation. The error is calculated as:

$$\mathrm{Error} = \frac{\{[((U)^{MP2}_{E_a^{red}=0} - (U)^{HDFT}_{E_a^{red}=0})\,(\mathrm{V})]^2 + [((E_a^{oxi})^{MP2}_{U_{red=0}} - (E_a^{oxi})^{HDFT}_{U_{red=0}})\,(\mathrm{eV})]^2\}^{1/2}}{2} + \frac{\{[((U)^{MP2}_{E_a^{oxi}=0} - (U)^{HDFT}_{E_a^{oxi}=0})\,(\mathrm{V})]^2 + [((E_a^{red})^{MP2}_{U_{oxi=0}} - (E_a^{red})^{HDFT}_{U_{oxi=0}})\,(\mathrm{eV})]^2\}^{1/2}}{2} \tag{9}$$

where MP2 and HDFT superscripts denote the level of theory at which the quantity is determined. This error is a measure of how well an HDFT method reproduces the semiquantitative MP2 results.

The results given in Table 1 and represented in Fig. 4 show that the smaller 6-31G(d,p) basis set gives more accurate results than the larger 6-31+G(d,p) basis set that includes diffuse functions for O. Although the 6-31+G(d,p) basis set is the recommended basis sets for use in kinetics studies using HDFT [56,57], as found earlier [26,17], the diffuse functions do not seem to be necessary when investigating oxygen reduction with the current

model. The use of the smaller basis set is also preferred because it is computationally more affordable. Accordingly, only the 6-31G(d,p) basis set was used in the Pt-catalyzed oxygen reduction study that is discussed below.

As the HF exchange contribution increases, the calculated activation energies (both for reduction and oxidation) increase and so does the difference ($U_{oxi=0} - U_{red=0}$). HDFT methods with small HF exchange contributions (e.g., B3PW91, B3LYP, PBE1PBE, and B1B95 for which $X < 30$) have higher errors that the methods in which $X = 40$–60. This seems to be due more to the smaller calculated activation energies rather than to big differences in $U_{red=0}$ or $U_{oxi=0}$. Comparing the HDFT methods based on Becke's exchange and the B95 correlation functionals that differ only by the HF exchange contributions (e.g., B1B95, BB1K, B1B95-50, and B1B95-60), one can see that the error has a minimum around $X = 50$ because it is higher for both BB1K and B1B95-60 than B1B95-50. Similar results are obtained for mPW1PW91 functional, but the errors (values of 0.52–0.53) are higher than those obtained for B1B95-50 functional (value of 0.38). Fig. 2 also shows that the B1B95-50 method gives results closest to the target MP2 results.

For the Pt-catalyzed study of ORR, we investigated only a subset of methods from the uncatalyzed study that includes mainly the methods with the smallest errors. For the Pt-catalyzed study, using all HDFT methods, it was found that the ground state of the oxidized form of the reaction model, $(H_2O)_2H_2O$–$H^+\cdots$OOPt, has a spin multiplicity of 3, and the reduced form of the reaction model, $(H_2O)_2H_2O\cdots$H–OOPt, has a spin multiplicity of 2. Comparing the HDFT results with the MP2 results, we investigate the same two points in activation energy versus electrochemical potential that include the same four important quantities. The errors are calculated again using Eq. (9). The results are given in Table 2 and are represented in Fig. 5. It was found that the smallest errors are obtained for B1B95-50 and mPW1PW91-60 methods.

Considering both the uncatalyzed and the Pt-catalyzed O_2 reduction and HOO oxidation, among the 25 investigated HDFT methods, the best results were obtained using the HDFT method based on Becke's exchange functional, B95 correlation functional, and a Hartree–Fock exchange contribution of 50% in conjunction with the 6-31G(d,p) basis set. This method is denoted B1B95-50/6-31G(d,p). Results of essentially equal accuracy were obtained using the HDFT method-based Becke's exchange functional, PW91 correlation functional, and a Hartree–Fock exchange contribution of 50% in conjunction with the 6-31G(d,p) basis set. This method is denoted B1PW91-50/6-31G(d,p). Both of these methods also give very accurate gas-phase bond energies for the oxygenated species. Based on the results obtained here, we propose these two methods to be used in studies of electrochemical oxygen reduction that uses larger electrode and reaction models.

5. Conclusions

The electrochemical processes occurring at the electrode surface are very challenging and especially difficult to model. The reaction models should contain a large number of atoms because they should include the reaction center, the electrode, and solvent molecules. In addition, electrochemical processes present another variable, the electrochemical potential, which needs to be included in the model. Oxygen reduction, the process occurring at the cathode of an electrolyte-based fuel cell, is one of the most important electrochemical processes. The study presented here focuses on developing accurate and computationally affordable methodologies to investigate this process.

The highly accurate ab initio methods are computationally too demanding for application to electrochemistry especially if the model for the electrode surface is large. Hybrid density functional theory presents an efficient alternative for studying these electrochemical processes because these methods are more affordable, accurate, and flexible in the choice of exchange and correlation functionals that one uses. This paper presents a procedure for obtaining hybrid density functional theory methods with specific reaction parameter that provide superior accuracy by optimizing the HF exchange contribution. Our interest is in obtaining HDFT methods that can be used for accurately investigating the process of oxygen reduction over platinum using large metal clusters.

In the present work, we have examined the performance of a variety of HDFT methods for the prediction of reversible potentials for oxygen reduction to water and potential-dependent activation energies of one-electron reduction of oxygen and oxidation of hydroperoxyl radical. The recommended basis sets for this type of calculations are 6-31G(d,p) for O and H and LANL2DZ for Pt. The results obtained here indicate that the inclusion of diffuse functions for oxygen by using the 6-31+G(d,p) basis set is unnecessary and less accurate. The HDFT methods with low HF exchange contributions show typically larger errors when compared with the semiquantitative results obtained with the MP2 method. These errors are a consequence of a systematic underestimation of the activation energies both for oxygen reduction and for hydroperoxyl oxidation. Among the HDFT methods investigated here, mPW1B95-50 and especially B1B95-50 show the smallest systematic errors for the reversible potential and uncatalyzed activation energies of oxygen reduction and hydroperoxyl oxidation. They also offer a superior performance for the Pt-catalyzed activation energies. The B1B95-50 method is particularly promising as a method that is affordable and accurate for studying oxygen reduction process on large platinum clusters.

The keywords to carry out B1B95-50 calculations (without Pt atoms) in Gaussian03 are BB95/6-31G(d,p) and IOp(3/76=0500005000). Similarly, the keywords to carry out mPW1B95-50 calculations in Gaussian03 are mPWB95/6-31G(d,p) and IOp(3/76=0500005000).

Acknowledgement

Oak Ridge Associated Universities through a Ralph Powe Junior Faculty Enhancement Award and Tennessee Technological University through a Faculty Research Initiation

Program are gratefully acknowledged for partially supported this research.

Appendix A

This appendix information contains:

- Fig. A.1 shows the schematics of the hydronium ion solvated with two water molecules and the label of hydrogen atoms used to describe its structure in Tables A.1 and A.2.
- Tables A.1 and A.2 give geometric parameters of the hydronium ion solvated with two water molecules used in this study obtained using the 6-31G(d,p) and 6-31+G(d,p) basis sets, respectively.
- Table A.3 gives the geometric parameters of the reduction precursor for the uncatalyzed oxygen reduction.
- Table A.4 gives the geometric parameters of the oxidation precursor for the uncatalyzed hydroperoxyl oxidation.

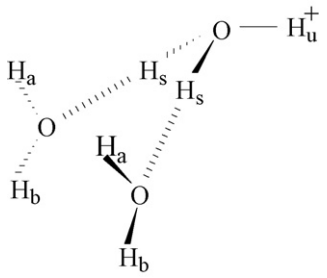

Fig. A.1. Schematics of the hydronium ion solvated with two water molecules and the label of hydrogen atoms used to describe its structure in Tables A.1 and A.2.

- Table A.5 gives the geometric parameters of the reduction precursor for the Pt-catalyzed oxygen reduction.
- Table A.6 gives the geometric parameters of the oxidation precursor for the Pt-catalyzed hydroperoxyl oxidation.

Table A.1
Internuclear distances, R (Å), and bond angles, θ (°), for different used models of the hydronium ion hydrogen-bonded with two water molecules, $(H_2O)_2H_2O–H^+$, calculated with different HDFT methods and the 6-31G(d,p) basis set

Method	R (O–H_u)	R (O–H_s)	θ (H_sOH_u)	θ (H_sOH_s)	R ($H_s\cdots OH_2$)	θ (OH_sO)	R (O–H_a)	R (O–H_b)	θ (H_sOH_a)	θ (H_sOH_b)	θ (H_aOH_b)
B3PW91	0.966	1.054	113.538	116.430	1.410	175.275	0.965	0.965	120.098	124.242	107.927
B3LYP	0.968	1.053	113.466	116.154	1.423	175.074	0.968	0.967	119.991	124.194	107.752
BH&HLYP	0.958	1.029	114.193	117.996	1.434	176.694	0.956	0.955	123.163	127.459	108.638
PBE1PBE	0.965	1.051	113.549	116.372	1.406	175.194	0.964	0.963	120.156	124.345	107.934
mPW1PW91	0.964	1.050	113.647	116.572	1.408	175.372	0.963	0.963	120.466	124.626	108.028
MPW1K	0.957	1.036	114.152	117.762	1.412	176.419	0.956	0.955	122.516	126.710	108.647
mPW1PW91-60	0.952	1.025	114.465	118.680	1.417	176.921	0.950	0.949	123.365	127.506	108.931
B1B95	0.965	1.047	113.518	116.373	1.425	175.405	0.964	0.963	120.652	124.911	107.855
BB1K	0.959	1.034	114.007	117.539	1.429	176.435	0.957	0.956	122.671	126.979	108.461
B1B95-50	0.956	1.028	114.149	118.056	1.431	176.748	0.954	0.953	123.241	127.547	108.639
B1B95-60	0.953	1.023	114.356	118.495	1.432	176.878	0.950	0.950	123.447	127.691	108.743
mPW1B95	0.963	1.043	113.744	116.735	1.422	175.626	0.961	0.961	121.256	125.528	108.070
MPWB1K	0.958	1.033	114.071	117.635	1.426	176.444	0.956	0.956	122.733	127.035	108.506
mPW1B95-50	0.956	1.029	114.173	118.030	1.427	176.699	0.954	0.953	123.172	127.473	108.641

The labels for hydrogen atoms are defined in Fig. A.1.

Table A.2
Internuclear distances, R (Å), and bond angles, θ (°), for different used models of the hydronium ion hydrogen-bonded with two water molecules, $(H_2O)_2H_2O–H^+$, calculated with different HDFT methods and the 6-31+G(d,p) basis set

Method	R (O–Hu)	R (O–Hs)	θ (HsOHu)	θ (HsOHs)	R ($H_s\cdots OH_2$)	θ (OH_sO)	R (O–H_a)	R (O–H_b)	θ (H_sOH_a)	θ (H_sOH_b)	θ (H_aOH_b)
B3PW91	0.967	1.049	113.954	118.060	1.421	176.194	0.966	0.965	123.033	126.959	108.792
B3LYP	0.970	1.047	114.094	118.356	1.436	176.279	0.968	0.967	123.399	127.319	108.790
BH&HLYP	0.959	1.027	114.597	118.863	1.446	176.674	0.957	0.957	123.627	127.474	108.879
PBE1PBE	0.966	1.046	113.971	117.981	1.417	176.156	0.964	0.964	123.079	127.024	108.790
mPW1PW91	0.965	1.045	114.027	118.168	1.419	176.278	0.964	0.963	123.231	127.164	108.841
MPW1K	0.958	1.033	114.314	118.643	1.423	176.599	0.957	0.956	123.523	127.422	108.961
mPW1PW91-60	0.953	1.023	114.588	118.865	1.426	176.783	0.951	0.950	123.557	127.401	109.020
B1B95	0.966	1.042	113.878	118.069	1.438	176.314	0.964	0.964	123.454	127.504	108.673
BB1K	0.960	1.031	114.222	118.497	1.441	176.547	0.958	0.957	123.598	127.583	108.774
mPW1B95	0.964	1.038	114.109	118.358	1.436	176.397	0.962	0.962	123.539	127.529	108.760
MPWB1K	0.959	1.030	114.348	118.608	1.438	176.571	0.957	0.957	123.599	127.540	108.817

The labels for hydrogen atoms are defined in Fig. A.1.

Table A.3
Internuclear distances (Å) and bond angle (°) for the reduction precursor of uncatalyzed oxygen reduction, $(H_2O)_2H_2O–H^+\cdots OO$, calculated with different HDFT methods

HDFT method/basis set	R ($H_2O\cdots OO$)	R ($H_2O–H^+$)	R ($H^+\cdots OO$)	R (O–O)	θ ($H^+\cdots O–O$)[a]
6-31G(d,p)					
B3PW91	3.044	0.970	2.073	1.209	105.34
B3LYP	3.003	0.973	2.030	1.216	105.15
BH&HLYP	2.991	0.962	2.029	1.191	105.66
PBE1PBE	2.991	0.969	2.022	1.204	105.45
mPW1PW91	3.015	0.968	2.046	1.204	105.42
MPW1K	3.015	0.961	2.054	1.189	105.74
mPW1PW91-60	3.011	0.955	2.056	1.177	106.01
B1B95	3.063	0.969	2.094	1.207	105.37
BB1K	3.052	0.962	2.090	1.192	105.70
B1B95-50	3.046	0.959	2.087	1.185	105.84
B1B95-60	3.037	0.956	2.081	1.178	106.00
mPW1B95	3.022	0.967	2.055	1.201	105.51
MPWB1K	3.020	0.962	2.058	1.190	105.75
mPW1B95-50	3.018	0.959	2.059	1.185	105.85
6-31G+(d,p)					
B3PW91	3.093	0.971	2.122	1.210	105.65
B3LYP	3.046	0.974	2.072	1.217	105.49
BH&HLYP	3.025	0.963	2.062	1.192	106.00
PBE1PBE	3.023	0.970	2.052	1.204	105.76
mPW1PW91	3.056	0.969	2.087	1.205	105.74
MPW1K	3.049	0.962	2.086	1.189	106.04
mPW1PW91-60	3.036	0.956	2.080	1.177	106.28
B1B95	3.116	0.970	2.147	1.207	105.69
BB1K	3.095	0.963	2.132	1.192	106.01
mPW1B95	3.064	0.968	2.096	1.201	105.83
MPWB1K	3.057	0.963	2.094	1.190	106.06

[a] This is the optimized angle in OOH.

Table A.4
Internuclear distances (Å) for the oxidation precursor of uncatalyzed hydroperoxyl oxidation, $(H_2O)_2H_2O\cdots H–OO$, calculated with different HDFT methods

HDFT method/basis set	R ($H_2O\cdots OO$)	R ($H_2O\cdots H$)	R (H–OO)	R (O–O)
6-31G(d,p)				
B3PW91	2.509	1.460	1.049	1.323
B3LYP	2.525	1.481	1.045	1.333
BH&HLYP	2.532	1.519	1.013	1.308
PBE1PBE	2.502	1.458	1.045	1.316
mPW1PW91	2.505	1.462	1.043	1.318
MPW1K	2.505	1.481	1.024	1.302
mPW1PW91-60	2.508	1.499	1.009	1.290
B1B95	2.526	1.488	1.039	1.320
BB1K	2.526	1.504	1.021	1.304
B1B95-50	2.526	1.512	1.014	1.297
B1B95-60	2.526	1.521	1.006	1.290
mPW1B95	2.520	1.487	1.033	1.313
MPWB1K	2.520	1.500	1.020	1.302
mPW1B95-50	2.521	1.507	1.015	1.297
6-31G+(d,p)				
B3PW91	2.532	1.492	1.040	1.324
B3LYP	2.551	1.514	1.037	1.335
BH&HLYP	2.558	1.551	1.008	1.309
PBE1PBE	2.526	1.490	1.036	1.317
mPW1PW91	2.528	1.493	1.035	1.318
MPW1K	2.529	1.512	1.017	1.302
mPW1PW91-60	2.531	1.528	1.003	1.290
B1B95	2.555	1.525	1.030	1.320
BB1K	2.554	1.540	1.014	1.304
mPW1B95	2.548	1.523	1.025	1.314
MPWB1K	2.548	1.535	1.013	1.302

Table A.5
Internuclear distances (Å) for the reduction precursor of Pt-catalyzed oxygen reduction, $(H_2O)_2H_2O–H^+\cdots OOPt$, calculated with different HDFT methods

HDFT method/basis set	R ($H_2O\cdots OO$)	R ($H_2O–H^+$)	R ($H^+\cdots OO$)	R (O–O)	R (Pt–O)[a]
B3PW91/6-31G(d,p)	2.648	0.999	1.649	1.297	1.853
BH&HLYP/6-31G(d,p)	2.686	0.977	1.709	1.283	1.915
MPW1K/6-31G(d,p)	2.689	0.977	1.712	1.274	1.903
mPW1PW91-60/6-31G(d,p)	2.659	0.972	1.687	1.268	1.899
B1B95-50/6-31G(d,p)	2.706	0.974	1.733	1.271	1.902
mPW1B95-50/6-31G(d,p)	2.698	0.974	1.724	1.271	1.901

[a] This is the optimized distance in Pt–OOH.

Table A.6
Internuclear distances (Å) for the oxidation precursor of Pt-catalyzed hydroperoxyl oxidation, $(H_2O)_2H_2O\cdots H–OOPt$, calculated with different HDFT methods

HDFT method/basis set	R ($H_2O\cdots OO$)	R ($H_2O–H$)	R ($H\cdots OO$)	R (O–O)	R (Pt–O)[a]
B3PW91/6-31G(d,p)	2.448	1.360	1.088	1.382	1.853
BH&HLYP/6-31G(d,p)	2.558	1.555	1.003	1.391	1.915
MPW1K/6-31G(d,p)	2.517	1.500	1.017	1.377	1.903
mPW1PW91-60/6-31G(d,p)	2.545	1.549	0.995	1.373	1.899
B1B95-50/6-31G(d,p)	2.550	1.546	1.004	1.377	1.902
mPW1B95-50/6-31G(d,p)	2.542	1.537	1.005	1.376	1.901

[a] This is the optimized distance in Pt–OOH.

References

[1] V. Jalan, E.J. Taylor, J. Electrochem. Soc. 130 (1983) 2299.
[2] M.T. Paffett, J.G. Berry, S. Gottesfeld, J. Electrochem. Soc. 135 (1988) 1431.
[3] S. Mukerjee, S. Srinivasan, J. Electroanal. Chem. 357 (1993) 201.
[4] S. Mukerjee, S. Srinivasan, M.P. Soriaga, J. McBreen, J. Electrochem. Soc. 142 (1995) 1409.
[5] T. Toda, H. Igarashi, H. Uchida, M. Watanabe, J. Electrochem. Soc. 146 (1999) 3750.
[6] M. Min, J. Cho, K. Cho, H. Kim, Electrochim. Acta 45 (2000) 4211.
[7] H. Yang, N. Alonso-Vante, J.-M. Leger, C. Lamy, J. Phys. Chem. B 108 (2004) 1938.
[8] H. Yang, W. Vogel, C. Lamy, N. Alonso-Vante, J. Phys. Chem. B 108 (2004) 11024.
[9] E. Antolini, R.R. Passos, E.A. Ticianelli, Electrochim. Acta 48 (2002) 263.
[10] U.A. Paulus, A. Wokaun, G.G. Scherer, T.J. Schmidt, V. Stamenkovic, N.M. Markovic, P.N. Ross, Electrochim. Acta 47 (2002) 3787.
[11] U.A. Paulus, A. Wokaun, G.G. Scherer, T.J. Schmidt, V. Stamenkovic, V. Radmilovic, N.M. Markovic, P.N. Ross, J. Phys. Chem. B 106 (2002) 4181.
[12] F.A. Uribe, T.A. Zawodzinski, Electrochim. Acta 47 (2002) 3799.
[13] V. Stamenkovic, T.J. Schmidt, P.N. Ross, N.M. Markovic, J. Phys. Chem. B 106 (2002) 11970.
[14] V. Stamenkovic, T.J. Schmidt, P.N. Ross, N.M. Markovic, J. Electroanal. Chem. 554–555 (2003) 191.
[15] V.S. Murthi, R.C. Urian, S. Mukerjee, J. Phys. Chem. B 108 (2004) 11011.
[16] J.O.M. Bockris, R. Abdu, J. Electroanal. Chem. 448 (1998) 189.
[17] A.B. Anderson, T.V. Albu, J. Electrochem. Soc. 147 (2000) 4229.
[18] R.A. Sidik, A.B. Anderson, J. Electroanal. Chem. 528 (2002) 69.
[19] C. Hartnig, M.T.M. Koper, J. Electroanal. Chem. 532 (2002) 165.
[20] T. Li, P.B. Balbuena, Chem. Phys. Lett. 367 (2003) 439.
[21] Y. Wang, P.B. Balbuena, J. Phys. Chem. B 108 (2004) 4376.
[22] Y. Wang, P.B. Balbuena, J. Phys. Chem. B 109 (2005) 14896.
[23] Y. Wang, P.B. Balbuena, J. Chem. Theory Comput. 1 (2005) 935.
[24] Y. Wang, P.B. Balbuena, J. Phys. Chem. B 109 (2005) 18902.
[25] D.S. Mainardi, S.R. Calvo, A.P.J. Jansen, J.J. Lukkien, P.B. Balbuena, Chem. Phys. Lett. 382 (2003) 553.
[26] A.B. Anderson, T.V. Albu, J. Am. Chem. Soc. 121 (1999) 11855.
[27] T.V. Albu, A.B. Anderson, Electrochim. Acta 46 (2001) 3001.
[28] T. Li, P.B. Balbuena, J. Phys. Chem. B 105 (2001) 9943.
[29] P.B. Balbuena, D. Altomare, L. Agapito, J.M. Seminario, J. Phys. Chem. B 107 (2003) 13671.
[30] P.B. Balbuena, D. Altomare, N. Vadlamani, S. Bingi, L.A. Agapito, J.M. Seminario, J. Phys. Chem. A 108 (2004) 6378.
[31] J.M. Seminario, L.A. Agapito, L. Yan, P.B. Balbuena, Chem. Phys. Lett. 410 (2005) 275.
[32] A. Panchenko, M.T.M. Koper, T.E. Shubina, S.J. Mitchell, E. Roduner, J. Electrochem. Soc. 151 (2004) A2016.
[33] Y. Xu, A.V. Ruban, M. Mavrikakis, J. Am. Chem. Soc. 126 (2004) 4717.
[34] J. Roques, A.B. Anderson, J. Electrochem. Soc. 151 (2004) E85.
[35] J. Roques, A.B. Anderson, J. Electrochem. Soc. 151 (2004) E340.
[36] J. Roques, A.B. Anderson, V.S. Murthi, S. Mukerjee, J. Electrochem. Soc. 152 (2005) E193.
[37] J. Roques, A.B. Anderson, J. Fuel Cell Sci. Technol. 2 (2005) 86.
[38] Z. Shi, J. Zhang, Z.-S. Liu, H. Wang, D.P. Wilkinson, Electrochim. Acta 51 (2006) 1905.
[39] B.J. Lynch, P.L. Fast, M. Harris, D.G. Truhlar, J. Phys. Chem. A 104 (2000) 4811.
[40] Y. Zhao, B.J. Lynch, D.G. Truhlar, J. Phys. Chem. A 108 (2004) 2715.
[41] Y. Zhao, D.G. Truhlar, J. Phys. Chem. A 108 (2004) 6908.
[42] J.O.M. Bockris, S.U.M. Khan, Surface Electrochemistry: A Molecular Level Approach, Plenum Press, New York, 1993, p. 493.
[43] A.B. Anderson, D.B. Kang, J. Phys. Chem. A 102 (1998) 5993.
[44] L.N. Kostadinov, A.B. Anderson, Electrochem. Solid State Lett. 6 (2003) E30.
[45] A.B. Anderson, Electrochim. Acta 48 (2003) 3743.
[46] A.B. Anderson, Y. Cai, R.A. Sidik, D.B. Kang, J. Electroanal. Chem. 580 (2005) 17.
[47] C. Lee, W. Yang, R.G. Parr, Phys. Rev. B 37 (1988) 785.
[48] A.D. Becke, J. Chem. Phys. 98 (1993) 5648.
[49] J.P. Perdew, M. Ernzerhof, K. Burke, J. Chem. Phys. 105 (1996) 9982.
[50] C. Adamo, V. Barone, J. Chem. Phys. 108 (1998) 664.
[51] A.D. Becke, J. Chem. Phys. 104 (1996) 1040.
[52] M.J. Frisch, G.W. Trucks, H.B. Schlegel, G.E. Scuseria, M.A. Robb, J.R. Cheeseman, J.A. Montgomery Jr., T. Vreven, K.N. Kudin, J.C. Burant, J.M. Millam, S.S. Iyengar, J. Tomasi, V. Barone, B. Mennucci, M. Cossi, G. Scalmani, N. Rega, G.A. Petersson, H. Nakatsuji, M. Hada, M. Ehara, K. Toyota, R. Fukuda, J. Hasegawa, M. Ishida, T. Nakajima, Y. Honda, O. Kitao, H. Nakai, M. Klene, X. Li, J.E. Knox, H.P. Hratchian, J.B. Cross, C. Adamo, J. Jaramillo, R. Gomperts, R.E. Stratmann, O. Yazyev, A.J. Austin, R.

Cammi, C. Pomelli, J.W. Ochterski, P.Y. Ayala, K. Morokuma, G.A. Voth, P. Salvador, J.J. Dannenberg, V.G. Zakrzewski, S. Dapprich, A.D. Daniels, M.C. Strain, O. Farkas, D.K. Malick, A.D. Rabuck, K. Raghavachari, J.B. Foresman, J.V. Ortiz, Q. Cui, A.G. Baboul, S. Clifford, J. Cioslowski, B.B. Stefanov, G. Liu, A. Liashenko, P. Piskorz, I. Komaromi, R.L. Martin, D.J. Fox, T. Keith, M.A. Al-Laham, C.Y. Peng, A. Nanayakkara, M. Challacombe, P.M.W. Gill, B. Johnson, W. Chen, M.W. Wong, C. Gonzalez, J.A. Pople, Gaussian03, Revision B.02, Gaussian, Inc., Pittsburgh, PA, 2003.

[53] B.N. Grgur, N.M. Markovic, P.N. Ross, Can. J. Chem. 75 (1997) 1465.

[54] D.B. Sepa, M.V. Vojnovic, L.M. Vracar, A. Damjanovic, Electrochim. Acta 31 (1986) 1105.

[55] C.R. Weast (Ed.), Handbook of Chemistry and Physics, 67th ed., CRC Press, Boca Raton, FL, 1986.

[56] B.J. Lynch, D.G. Truhlar, J. Phys. Chem. A 105 (2001) 2936.

[57] B.J. Lynch, Y. Zhao, D.G. Truhlar, J. Phys. Chem. A 107 (2003) 1384.